RAA 2016 Vol. **16** No. **11**, 173 (10pp) doi: 10.1088/1674–4527/16/11/173

http://www.raa-journal.org *http://iopscience.iop.org/raa*

***R**esearch in*
***A**stronomy and*
***A**strophysics*

What determines the observational differences of blazars?

Xu-Liang Fan[1,2,3], Jin-Ming Bai[1,2] and Ji-Rong Mao[1,2]

[1] Yunnan Observatories, Chinese Academy of Sciences, Kunming 650011, China; *fxl1987@ynao.ac.cn, baijinming@ynao.ac.cn*
[2] Key Laboratory for the Structure and Evolution of Celestial Objects, Chinese Academy of Sciences, Kunming 650011, China
[3] University of Chinese Academy of Sciences, Beijing 100049, China

Received 2016 May 30; accepted 2016 July 18

Abstract We examine the scenario that the Doppler factor determines the observational differences of blazars. Significantly negative correlations are found between the observational synchrotron peak frequency and the Doppler factor. After correcting the Doppler boosting, the intrinsic peak frequency has a tight linear relation with the Doppler factor. It is interesting that this relation is consistent with the scenario that the black hole mass governs both the bulk Lorentz factor and the synchrotron peak frequency. In addition, the distinction between the kinetic jet powers of BL Lac objects and flat spectrum radio quasars disappears after the boosting factor δ^2 is considered. The negative correlation between the peak frequency and the observational isotropic luminosity, known as the blazar sequence, also disappears after the Doppler boosting is corrected. We also find that the correlation between the Compton dominance and the Doppler factor exists for all types of blazars. Therefore, this correlation is unsuitable for examining the external Compton emission dominance.

Key words: galaxies: jets — BL Lacertae objects: general — quasars: general — radiation mechanisms: non-thermal

1 INTRODUCTION

Blazars are the most extreme subclass of active galactic nuclei (AGNs). Their radiation is dominated by the non-thermal emission of a relativistic jet having a small viewing angle with respect to our line of sight. The spectral energy distributions (SEDs) of blazars show two peaks (in the $\nu - \nu L_\nu$ diagram) which are believed to be produced by synchrotron and inverse Compton (IC) processes, respectively. However, whether external photons outside the jet participate in the IC process is still an open question (e.g., Chen & Bai 2011; Meyer et al. 2012).

Blazars are classified as flat spectrum radio quasars (FSRQs) and BL Lac objects (BL Lacs) by their optical spectra. They can also be classified as low synchrotron peaked blazars (LSPs), intermediate synchrotron peaked blazars (ISPs) and high synchrotron peaked blazars (HSPs) based on the synchrotron peak frequency (Abdo et al. 2010). An alternative classification based on the ratio of broad line luminosity to Eddington luminosity was proposed by Ghisellini et al. (2011). This classification considers the potential selection effect on the equivalent width (EW) measurement of broad lines due to the Doppler boosting effect, and links the observational classification to accretion regimes. On the other hand, the blazar sequence based on bolometric luminosity was put forward to unify the observational differences of blazars (Fossati et al. 1998). The negative correlations between the peak frequency and luminosity, as well as the Compton dominance (CD), are explained as increased cooling from external photons outside the jet with increasing luminosity (Ghisellini et al. 1998). However, later studies showed that the blazar sequence was an artefact of Doppler boosting (Nieppola et al. 2008) or redshift selection effects (Giommi et al. 2012), and sources with both high luminosity and high peak frequency which break the blazar sequence exist (e.g., Padovani et al. 2012; Ackermann et al. 2015). To improve the simple blazar sequence, Meyer et al. (2011) proposed a concept named "blazar envelope" which considered the jet power and the orientation effect. According to the blazar envelope, blazars are composed of two populations divided by jet power, and an envelope forms due to different orientations for various sources.

Since its launch in 2008, the Large Area Telescope (LAT) onboard the Fermi Gamma-ray Space Telescope (Fermi) has detected 1444 AGNs in the Third LAT AGN catalog (3LAC) clean sample (Ackermann et al. 2015). The broad energy range and high accuracy of LAT promote deep understandings of both the radiation mechanism (e.g. Chen & Bai 2011; Meyer et al. 2012) and the classification of blazars (e.g. Ghisellini et al. 2009, 2011). However, it is still uncertain if the differences in blazars are determined

by their different physical features or by observational effects (such as their orientation). Moreover, it also needs to be verified if there are one or more factors that affect blazar classifications.

Distinctions in Doppler boosting have been discovered for different subclasses of blazars, such as BL Lacs and FSRQs (Hovatta et al. 2009), or X-ray-selected BL Lacs and radio-selected BL Lacs (Ghisellini et al. 1993). Stronger Doppler boosting was also suggested to explain γ-ray detected blazars by many papers (e.g. Kovalev et al. 2009; Lister et al. 2009a; Savolainen et al. 2010; Lister et al. 2015). Furthermore, the blazar sequence was found to be an artefact of Doppler boosting (Nieppola et al. 2008). These results indicate that the observational differences shown by blazars could be determined by the Doppler factor. Thus, this work aims to identify this scenario. Our paper is organized as follows. In Section 2, we examine the connection between the Doppler factor and the synchrotron peak frequency. Section 3 presents the impact on jet power due to the Doppler factor. The Doppler-corrected blazar sequence is discussed in Section 4. In Section 5, we recheck its validity by examining the external Compton (EC) dominance with the correlation between CD and Doppler factor. Discussions are presented in Section 6. In this paper, we use a ΛCDM cosmology model with $h = 0.71, \Omega_m = 0.27$ and $\Omega_\Lambda = 0.73$ (Komatsu et al. 2009).

2 SYNCHROTRON PEAK FREQUENCY VERSUS DOPPLER FACTOR

The SED classification of blazars is based on the synchrotron peak frequency. The synchrotron peak frequency, $\nu_{\rm S,p} \propto \gamma_{\rm b}^2 B\delta$, is related to the electron distribution and the magnetic field strength of the emission region (where $\gamma_{\rm b}$ is the break energy of the electron spectrum, B is the magnetic field strength and δ is the Doppler factor; see e.g. Tavecchio et al. 1998). In order to constrain the effect on blazar classification due to the Doppler factor, we first examine the correlation between Doppler factor and synchrotron peak frequency. Because the Doppler factor is determined by both the bulk Lorentz factor and the viewing angle ($\delta = [\Gamma(1 - \beta\cos\theta)]^{-1}$, where β is the bulk velocity in the unit of the speed of light, Γ is the bulk Lorentz factor of a relativistic jet and θ is the viewing angle), the wide distribution of these two parameters for both high and low peaked sources has a major impact on the correlation between peak frequency and Doppler factor. Many studies have demonstrated that γ-ray detected sources exhibit smaller viewing angles (e.g. Savolainen et al. 2010). Thus, less aligned sources are generally excluded from a γ-ray selected sample. For such a sample, the Doppler factor is mainly determined by an intrinsic feature of jet physics, i.e. the bulk Lorentz factor. Therefore, throughout this paper, we just deal with the γ-ray selected samples and the approximation $\delta \sim \Gamma \sim 1/\theta$ is used.

2.1 Parameter Estimations

The 3LAC provides an ideal γ-ray data set to cross-match with samples in other bands. In the 3LAC, Ackermann et al. (2015) listed the synchrotron peak frequency estimated by the third-degree polynomial fit. Meanwhile, another method based on the empirical relations proposed by Abdo et al. (2010) was often used in related literatures. Ackermann et al. (2015) compared these two methods and concluded that the average offset between the peak frequencies estimated by these two methods was less than 0.26 dex. Because we need to estimate the bolometric luminosity and CD in the following sections, we use the empirical relations in Abdo et al. (2010) to estimate the synchrotron peak frequency throughout this paper. The k-correction is applied as $\nu_{\rm S,p} = \nu_{\rm S,p}^{'}(1+z)$. The Doppler-corrected intrinsic peak frequency is calculated with $\nu_{\rm S,int} = \nu_{\rm S,p}/\delta$. Because the estimation of Doppler factor has large uncertainties and strong dependence on the observational epoch and frequency (Lähteenmäki & Valtaoja 1999), we use two groups of Doppler factors estimated through two independent methods in this paper. These two groups of results can be cross-checked. For the first method, the brightness temperature is obtained by fitting the variability timescale of radio flux (Lähteenmäki & Valtaoja 1999), then the Doppler factor is calculated as $(T_{\rm var}/T_{\rm eq})^{1/3}$ (hereafter $\delta_{\rm var}$), where $T_{\rm eq} = 5 \times 10^{10}\,{\rm K}$ is the equipartition brightness temperature (Readhead 1994). For the other method, the core brightness temperature is obtained by fitting the minimum observable size (Readhead 1994), then $\delta = T_{\rm core}/T_{\rm eq}$ (hereafter $\delta_{\rm eq}$).

Considering the possible variability of the Doppler factors, we search the archive for the Doppler factor during the Fermi era. $\delta_{\rm var}$ is derived from Hovatta et al. (2009). Hovatta et al. (2009) estimated $\delta_{\rm var}$ for 89 objects (two objects were added from Savolainen et al. 2010). Among them, 62 have redshift measurements and estimations of $\nu_{\rm S,p}$ in the 3LAC clean sample. There are 39 FSRQs, 16 LSP-BL Lacs (LBLs), four ISP BL Lacs (IBLs), one HSP-BL Lacs (HBLs) and two AGNs of other types in this cross-matched sample. Linford et al. (2012) observed 232 AGNs with the Very Long Baseline Array at 5 GHz from 2009 to 2010, and obtained their core brightness temperature. We estimate $\delta_{\rm eq}$ with the method described above. $\nu_{\rm S,p}$ is obtained for 139 sources from this sample. Of these 139 sources, there are 85 FSRQs, 19 LBLs, 13 IBLs, 16 HBLs and six AGNs of other types. The details of these two samples are listed in Table 1. The two groups of Doppler factors have very different distributions (Fig. 1), and values of $\delta_{\rm var}$ are larger than those of $\delta_{\rm eq}$ to some extent. $\delta_{\rm var}$ is derived from long term radio monitoring. The targets for monitoring are biased toward brighter and more variable sources (Lister et al. 2009b), which makes HBLs and IBLs rare in that sample. Therefore, the sources with $\delta_{\rm var}$ tend to have large Doppler factors. On the other hand, $\delta_{\rm eq}$ estimation is only reliable for low redshift sources, and

Table 1 Source Data

3FGL name	z	opt.	SED	$\nu_{\rm S,p}$	CD	$\delta_{\rm var}$	$\nu_{\rm S,int}$	$L_{\rm bol}$	$P_{\rm j,int}$	$\delta_{\rm eq}$	$\nu_{\rm S,int}$	$L_{\rm bol}$	$P_{\rm j,int}$
(1)	(2)	(3)	(4)	(5)	(6)	(7)	(8)	(9)	(10)	(11)	(12)	(13)	(14)
J0006.4+3825	0.23	FSRQ	LSP	13.58	0.77	-	-	-	-	−0.14	13.72	46.25	-
J0050.6−0929	0.63	BL Lac	ISP	14.88	−0.74	0.98	13.90	39.38	42.35	-	-	-	-
J0058.3+3315	1.37	FSRQ	LSP	13.51	0.45	-	-	-	-	0.73	12.79	41.10	-
J0108.7+0134	2.10	FSRQ	LSP	13.50	0.37	1.26	12.24	38.78	43.93	-	-	-	-
J0109.1+1816	0.44	BL Lac	HSP	15.96	−1.28	-	-	-	-	−0.49	16.45	48.96	-
J0112.1+2245	0.26	BL Lac	ISP	15.02	−0.33	0.96	14.06	38.57	41.83	0.02	15.00	45.11	43.70
J0112.8+3207	0.60	FSRQ	ISP	14.86	−0.22	-	-	-	-	−0.08	14.95	46.84	45.37
J0113.4+4948	0.39	FSRQ	LSP	13.26	−0.15	-	-	-	-	−0.16	13.42	46.14	-
J0137.0+4752	0.86	FSRQ	LSP	13.63	0.14	1.32	12.31	37.15	42.15	0.72	12.91	41.34	43.34
J0151.6+2205	1.32	FSRQ	LSP	13.45	0.68	0.71	12.74	42.09	-	-	-	-	-
J0204.8+3212	1.47	FSRQ	LSP	13.76	2.57	-	-	-	-	1.40	12.36	39.14	42.53
J0217.5+7349	2.37	FSRQ	LSP	13.90	2.17	0.93	12.97	43.02	43.15	0.41	13.49	46.67	44.19
J0221.1+3556	0.94	FSRQ	LSP	-	-	-	-	-	-	−1.17	-	-	47.91
J0222.6+4301	0.44	BL Lac	HSP	14.83	−0.51	0.41	14.41	43.42	44.60	-	-	-	-
J0237.9+2848	1.21	FSRQ	LSP	13.39	0.56	1.21	12.19	38.69	43.18	0.48	12.92	43.79	44.64
J0238.6+1636	0.94	BL Lac	LSP	13.86	−0.04	1.38	12.48	37.02	41.96	0.42	13.43	43.71	43.87
J0245.4+2410	2.24	FSRQ	LSP	13.36	1.07	-	-	-	-	−1.26	14.62	56.33	-
J0310.8+3814	0.94	FSRQ	LSP	13.96	0.15	-	-	-	-	0.71	13.25	41.03	-
J0325.2+3410	0.06	NLSY1	HSP	15.23	1.13	-	-	-	-	−0.37	15.59	47.77	-
J0325.5+2223	2.07	FSRQ	LSP	13.41	1.61	-	-	-	-	0.44	12.97	44.96	-
J0339.5−0146	0.85	FSRQ	LSP	13.40	0.24	1.24	12.16	37.91	42.83	-	-	-	-
J0423.2−0119	0.92	FSRQ	LSP	13.67	−0.08	1.30	12.37	37.58	42.64	-	-	-	-
J0433.6+2905	0.97	BL Lac	LSP	14.99	−0.51	-	-	-	-	−0.08	15.07	47.05	-
J0449.0+1121	2.15	FSRQ	LSP	13.81	1.02	-	-	-	-	0.39	13.41	45.14	44.43
J0501.2−0157	2.29	FSRQ	LSP	13.18	0.35	1.20	11.98	39.09	43.90	-	-	-	-
J0509.3+1012	0.62	FSRQ	LSP	13.71	0.66	-	-	-	-	−0.10	13.81	46.78	-
J0510.0+1802	0.42	FSRQ	LSP	13.26	0.35	-	-	-	-	−0.14	13.40	46.38	-
J0530.8+1330	2.07	FSRQ	LSP	13.27	0.97	1.49	11.77	37.32	42.93	0.43	12.84	44.79	45.06
J0608.0−0835	0.87	FSRQ	ISP	13.98	−0.28	0.88	13.10	40.40	43.66	-	-	-	-
J0612.8+4122	-	BL Lac	ISP	-	-	-	-	-	-	0.02	-	-	43.70
J0638.6+7324	1.85	FSRQ	LSP	13.62	0.72	-	-	-	-	−0.02	13.65	47.59	-
J0650.7+2503	0.20	BL Lac	HSP	16.32	−0.72	-	-	-	-	−1.15	17.48	53.13	-
J0654.4+4514	0.93	FSRQ	LSP	-	-	-	-	-	-	−0.48	-	-	46.05
J0654.4+5042	1.25	FSRQ	ISP	14.37	−0.25	-	-	-	-	−0.34	14.71	48.58	44.29
J0710.5+4732	1.29	BL Lac	ISP	14.37	0.37	-	-	-	-	0.12	14.25	46.40	45.35
J0712.6+5033	0.50	BL Lac	LSP	13.66	0.06	-	-	-	-	0.09	13.57	44.48	-
J0719.3+3307	0.78	FSRQ	ISP	13.80	0.52	-	-	-	-	0.30	13.50	43.90	-
J0721.9+7120	0.13	BL Lac	LSP	14.56	0.07	1.04	13.52	37.52	42.69	1.17	13.39	36.59	42.42
J0725.2+1425	1.04	FSRQ	ISP	13.60	0.28	-	-	-	-	−0.12	13.72	47.43	-
J0738.1+1741	0.42	BL Lac	LSP	14.16	−0.67	0.58	13.58	41.85	43.31	−0.55	14.72	49.78	45.58
J0739.4+0137	0.19	FSRQ	ISP	13.58	0.29	0.93	12.64	38.64	42.23	-	-	-	-
J0742.6+5444	0.72	FSRQ	ISP	13.85	0.50	-	-	-	-	0.95	12.89	39.32	-
J0746.4+2540	2.98	FSRQ	LSP	13.50	3.10	-	-	-	-	0.88	12.62	43.65	-
J0750.6+1232	0.89	FSRQ	LSP	13.49	−0.16	-	-	-	-	0.82	12.67	40.55	-
J0757.0+0956	0.27	BL Lac	LSP	14.37	−0.78	0.75	13.62	39.98	42.84	-	-	-	-
J0805.4+6144	3.03	FSRQ	LSP	13.27	1.76	-	-	-	-	0.02	13.24	48.47	-
J0809.6+3456	0.08	BL Lac	HSP	15.45	−1.36	-	-	-	-	−0.42	15.87	47.01	-
J0809.8+5218	0.14	BL Lac	HSP	15.66	−0.53	-	-	-	-	−1.25	16.91	53.40	45.79
J0814.7+6428	0.24	BL Lac	LSP	14.32	0.39	-	-	-	-	0.16	14.16	43.48	-
J0816.7+5739	-	BL Lac	HSP	-	-	-	-	-	-	−2.00	-	-	48.01
J0818.2+4223	0.53	BL Lac	LSP	13.57	−0.03	0.66	12.91	41.11	43.08	0.80	12.77	40.14	42.81
J0824.9+5551	1.42	FSRQ	LSP	13.50	0.58	-	-	-	-	−0.12	13.62	48.01	-
J0830.7+2408	0.94	FSRQ	LSP	13.73	1.01	1.12	12.61	39.18	42.99	0.92	12.81	40.57	43.38
J0834.1+4223	0.25	FSRQ	ISP	13.82	0.26	-	-	-	-	−0.11	13.92	45.48	44.40
J0841.4+7053	2.22	FSRQ	LSP	13.47	1.98	1.21	12.26	40.79	43.55	−0.71	14.17	54.21	47.38
J0850.2−1214	0.57	FSRQ	LSP	13.72	0.26	1.22	12.51	37.06	-	-	-	-	-
J0854.8+2006	0.31	BL Lac	LSP	14.20	−0.42	1.23	12.97	36.89	41.71	0.80	13.39	39.89	42.57
J0915.8+2933	-	BL Lac	HSP	-	-	-	-	-	-	−0.59	-	-	44.93
J0920.9+4442	2.19	FSRQ	LSP	13.72	0.38	-	-	-	-	−0.14	13.87	48.43	46.13
J0921.8+6215	1.45	FSRQ	LSP	13.51	0.30	-	-	-	-	0.50	13.01	43.32	44.66

Column (1) is the source name in the third Fermi-LAT catalog (3FGL, Acero et al. 2015). Columns (2)–(4) give the redshift, optical type and the SED classification in the 3LAC respectively. Column (5) and Column (6) are the k-corrected synchrotron peak frequency in the unit of Hz and the CD respectively. Column (7) is the Doppler factor estimated from radio variability. Columns (8)–(10) are the Doppler-corrected intrinsic synchrotron peak frequency in the unit of Hz, intrinsic luminosity in the unit of erg s^{-1} and intrinsic jet power in the unit of erg s^{-1} calculated with $\delta_{\rm var}$ respectively. Column (11) is the Doppler factor derived from VLBI observations. Columns (12)–(14) are the Doppler-corrected intrinsic synchrotron peak frequency in the unit of Hz, intrinsic luminosity in the unit of erg s^{-1} and intrinsic jet power in the unit of erg s^{-1} calculated with $\delta_{\rm eq}$ respectively. All of the values except redshift are in logarithmic space.

Table 1 — *Continued.*

3FGL name	z	opt.	SED	$\nu_{\rm S,p}$	CD	$\delta_{\rm var}$	$\nu_{\rm S,int}$	$L_{\rm bol}$	$P_{\rm j,int}$	$\delta_{\rm eq}$	$\nu_{\rm S,int}$	$L_{\rm bol}$	$P_{\rm j,int}$
(1)	(2)	(3)	(4)	(5)	(6)	(7)	(8)	(9)	(10)	(11)	(12)	(13)	(14)
J0929.4+5013	-	BL Lac	ISP	-	-	-	-	-	-	−0.02	-	-	44.13
J0937.7+5008	0.28	FSRQ	LSP	13.62	0.01	-	-	-	-	0.32	13.29	42.18	-
J0945.9+5756	0.23	BL Lac	ISP	14.36	−0.12	-	-	-	-	−0.48	14.84	47.79	44.79
J0948.6+4041	1.25	FSRQ	LSP	13.51	0.50	0.81	12.71	41.39	44.04	-	-	-	-
J0957.6+5523	0.90	FSRQ	ISP	13.38	−0.15	-	-	-	-	−1.70	15.08	58.42	48.96
J0958.6+6534	0.37	BL Lac	LSP	14.15	−0.20	0.79	13.35	39.90	42.84	1.01	13.14	38.41	42.41
J1012.6+2439	1.80	FSRQ	LSP	13.86	0.83	-	-	-	-	−0.95	14.81	53.44	-
J1015.0+4925	0.21	BL Lac	HSP	15.53	−0.49	-	-	-	-	−0.80	16.33	50.84	-
J1033.2+4116	1.12	FSRQ	LSP	13.28	0.29	-	-	-	-	1.65	11.63	34.66	42.06
J1033.8+6051	1.40	FSRQ	LSP	13.66	0.37	-	-	-	-	−0.51	14.17	50.21	46.53
J1037.5+5711	-	BL Lac	ISP	-	-	-	-	-	-	−0.46	-	-	44.26
J1043.1+2407	0.56	FSRQ	LSP	14.72	−0.76	-	-	-	-	0.40	14.32	42.89	-
J1048.4+7144	1.15	FSRQ	LSP	13.69	0.45	-	-	-	-	0.34	13.35	44.35	-
J1058.5+0133	0.89	BL Lac	LSP	13.52	−0.20	1.09	12.43	38.98	43.44	-	-	-	-
J1058.6+5627	0.14	BL Lac	HSP	15.04	−0.44	-	-	-	-	−0.41	15.45	47.37	44.51
J1104.4+3812	0.03	BL Lac	HSP	16.43	−0.56	-	-	-	-	0.22	16.21	42.68	42.83
J1105.9+2814	0.84	FSRQ	LSP	13.91	0.59	-	-	-	-	0.65	13.25	41.58	-
J1112.4+3449	1.96	FSRQ	LSP	13.83	0.64	-	-	-	-	0.11	13.73	46.12	-
J1117.0+2014	0.14	BL Lac	HSP	16.35	−1.07	-	-	-	-	−0.59	16.94	48.83	-
J1124.1+2337	1.55	FSRQ	LSP	13.26	0.32	-	-	-	-	0.14	13.11	45.55	-
J1136.6+7009	0.05	BL Lac	HSP	15.87	−1.38	-	-	-	-	−0.30	16.17	45.97	44.08
J1150.3+2417	0.18	BL Lac	ISP	13.68	−0.45	-	-	-	-	−0.05	13.73	44.83	-
J1151.4+5858	-	BL Lac	ISP	-	-	-	-	-	-	−1.11	-	-	46.12
J1154.3+6023	1.12	FSRQ	LSP	13.71	1.58	-	-	-	-	0.90	12.81	40.65	42.72
J1159.5+2914	0.73	FSRQ	LSP	13.25	0.20	1.45	11.79	36.08	42.52	1.67	11.57	34.54	42.08
J1203.1+6029	0.07	BL Lac	ISP	14.65	−0.65	-	-	-	-	−0.26	14.91	45.26	43.97
J1209.4+4119	-	BL Lac	LSP	-	-	-	-	-	-	−0.24	-	-	43.62
J1217.8+3007	0.13	BL Lac	HSP	15.86	−0.99	-	-	-	-	0.17	15.70	43.88	43.58
J1220.2+7105	0.45	FSRQ	ISP	-	-	-	-	-	-	0.30	-	-	44.06
J1221.4+2814	0.10	BL Lac	ISP	14.20	−0.38	0.08	14.12	43.68	41.98	−0.14	14.34	45.19	42.42
J1224.6+4332	-	BL Lac	LSP	-	-	-	-	-	-	−0.20	-	-	46.14
J1224.9+2122	0.44	FSRQ	LSP	13.78	0.57	0.72	13.06	41.29	43.95	0.90	12.88	40.00	43.58
J1229.1+0202	0.16	FSRQ	LSP	13.34	0.52	1.23	12.11	37.75	43.04	-	-	-	-
J1230.3+2519	0.14	BL Lac	ISP	14.89	−0.64	-	-	-	-	−0.40	15.30	47.16	-
J1231.7+2847	0.24	BL Lac	ISP	15.19	−0.44	-	-	-	-	−0.58	15.77	48.86	46.37
J1243.1+3627	-	BL Lac	HSP	-	-	-	-	-	-	−0.76	-	-	45.23
J1248.2+5820	-	BL Lac	ISP	-	-	-	-	-	-	−0.11	-	-	44.73
J1253.2+5300	-	BL Lac	LSP	-	-	-	-	-	-	−0.24	-	-	44.64
J1256.1−0547	0.54	FSRQ	LSP	12.87	0.48	1.38	11.49	36.92	42.97	-	-	-	-
J1258.1+3233	0.81	FSRQ	LSP	13.42	0.20	-	-	-	-	−0.16	13.57	47.10	-
J1303.0+2435	0.99	BL Lac	LSP	14.03	0.30	-	-	-	-	0.48	13.55	42.55	-
J1308.7+3545	1.05	FSRQ	LSP	13.37	0.25	-	-	-	-	0.81	12.56	40.20	-
J1310.6+3222	1.00	FSRQ	LSP	13.53	−0.12	1.19	12.34	38.17	42.99	1.12	12.41	38.65	43.13
J1312.7+4828	0.64	AGN	LSP	13.17	0.74	-	-	-	-	−1.49	14.67	56.10	-
J1317.8+3429	1.05	FSRQ	LSP	13.53	0.36	-	-	-	-	−0.05	13.58	46.70	45.65
J1326.8+2211	1.40	FSRQ	LSP	13.43	0.47	1.33	12.10	37.56	42.46	1.39	12.04	37.13	42.34
J1331.8+4718	0.67	FSRQ	LSP	14.35	0.17	-	-	-	-	0.41	13.94	42.97	-
J1333.7+5057	1.36	FSRQ	ISP	14.13	1.07	-	-	-	-	−0.53	14.67	50.35	-
J1337.6−1257	0.54	FSRQ	LSP	13.37	−0.13	0.92	12.45	39.54	43.31	-	-	-	-
J1345.6+4453	2.53	FSRQ	LSP	13.55	1.04	-	-	-	-	0.63	12.92	43.15	-
J1350.8+3035	0.71	FSRQ	LSP	13.87	0.15	-	-	-	-	−0.18	14.06	47.08	-
J1357.6+7643	1.59	FSRQ	LSP	13.08	0.44	-	-	-	-	0.23	12.85	45.02	-
J1359.0+5544	1.01	FSRQ	ISP	13.53	1.35	-	-	-	-	0.10	13.43	45.89	-
J1416.0+1325	0.25	BCU I	LSP	13.55	−0.55	1.09	12.46	37.22	-	-	-	-	-
J1419.9+5425	0.15	BL Lac	LSP	13.98	−0.54	0.71	13.27	39.51	42.37	-	-	-	-
J1427.0+2347	-	BL Lac	HSP	-	-	-	-	-	-	−0.62	-	-	45.45
J1434.1+4203	1.24	FSRQ	LSP	-	-	-	-	-	-	−0.52	-	-	46.39
J1436.8+2322	1.54	FSRQ	LSP	13.49	−0.17	-	-	-	-	0.75	12.74	41.35	-
J1438.7+3710	2.40	FSRQ	LSP	12.95	0.86	-	-	-	-	0.66	12.29	42.43	-
J1443.9+2502	0.94	FSRQ	-	13.42	−0.19	-	-	-	-	0.36	13.06	43.20	-
J1454.5+5124	-	BL Lac	ISP	-	-	-	-	-	-	−0.93	-	-	47.13
J1504.4+1029	1.84	FSRQ	LSP	13.49	0.75	1.08	12.41	40.09	43.49	−0.15	13.64	48.70	45.95
J1506.1+3728	0.67	FSRQ	LSP	12.89	0.35	-	-	-	-	0.23	12.66	44.19	-
J1512.8−0906	0.36	FSRQ	LSP	13.58	0.96	1.22	12.36	37.89	42.48	-	-	-	-
J1516.9+1926	-	BL Lac	LSP	-	-	-	-	-	-	0.66	-	-	42.75
J1522.1+3144	1.49	FSRQ	LSP	13.42	1.58	-	-	-	-	0.35	13.07	45.09	-
J1539.5+2746	2.19	FSRQ	ISP	14.21	−0.31	-	-	-	-	0.29	13.93	44.65	-
J1540.8+1449	0.61	BL Lac	LSP	13.58	−0.81	0.63	12.94	41.32	43.99	-	-	-	-
J1542.9+6129	-	BL Lac	ISP	-	-	-	-	-	-	−0.32	-	-	43.83

Table 1 — *Continued.*

3FGL name	z	opt.	SED	$\nu_{\rm S,p}$	CD	$\delta_{\rm var}$	$\nu_{\rm S,int}$	$L_{\rm bol}$	$P_{\rm j,int}$	$\delta_{\rm eq}$	$\nu_{\rm S,int}$	$L_{\rm bol}$	$P_{\rm j,int}$
(1)	(2)	(3)	(4)	(5)	(6)	(7)	(8)	(9)	(10)	(11)	(12)	(13)	(14)
J1553.5+1256	1.31	FSRQ	ISP	13.80	0.15	-	-	-	-	−0.62	14.42	51.10	46.75
J1604.6+5714	0.72	FSRQ	ISP	13.70	0.41	-	-	-	-	−0.69	14.39	50.93	-
J1607.0+1551	0.50	FSRQ	LSP	13.36	0.17	-	-	-	-	−0.20	13.56	46.84	45.21
J1608.6+1029	1.23	FSRQ	LSP	13.39	0.98	1.40	11.99	37.53	42.49	−0.08	13.47	47.90	45.46
J1613.8+3410	1.40	FSRQ	LSP	13.43	−0.80	1.14	12.29	38.95	43.03	−0.15	13.57	47.93	45.59
J1630.6+8232	0.02	RDG	LSP	14.29	−0.94	-	-	-	-	−0.55	14.84	46.59	-
J1635.2+3809	1.81	FSRQ	LSP	13.45	0.74	1.33	12.12	38.44	42.96	-	-	-	-
J1637.7+4715	0.74	FSRQ	LSP	13.06	0.32	-	-	-	-	0.18	12.88	44.75	45.06
J1637.9+5719	0.75	FSRQ	ISP	13.47	1.37	1.15	12.33	39.16	-	-	-	-	-
J1640.9+1142	0.08	BCU I	ISP	13.93	−0.60	-	-	-	-	−0.82	14.75	49.17	-
J1642.9+3950	0.59	FSRQ	LSP	13.60	−0.29	0.89	12.71	40.26	43.96	-	-	-	-
J1647.4+4950	0.05	BCU I	LSP	14.68	0.22	-	-	-	-	−0.39	15.07	46.25	-
J1656.9+6008	0.62	FSRQ	ISP	13.63	0.82	-	-	-	-	0.16	13.47	44.93	-
J1700.1+6829	0.30	FSRQ	LSP	13.36	0.87	-	-	-	-	0.16	13.20	44.15	44.04
J1709.6+4318	1.03	FSRQ	LSP	13.97	0.79	-	-	-	-	−0.36	14.33	48.88	-
J1719.2+1744	0.14	BL Lac	LSP	13.32	−0.27	-	-	-	-	0.52	12.79	40.32	42.51
J1722.7+1014	0.73	FSRQ	LSP	13.53	0.17	-	-	-	-	−0.41	13.94	48.78	-
J1727.1+4531	0.72	FSRQ	LSP	13.70	0.52	-	-	-	-	1.53	12.18	35.71	42.04
J1728.3+5013	0.06	BL Lac	HSP	15.98	−1.42	-	-	-	-	−0.86	16.84	49.94	45.00
J1728.5+0428	0.29	FSRQ	LSP	13.82	0.62	0.58	13.24	41.49	43.02	-	-	-	-
J1730.6+3711	0.20	BL Lac	ISP	14.68	−0.80	-	-	-	-	−1.42	16.10	54.18	-
J1733.0−1305	0.90	FSRQ	LSP	12.44	0.36	1.03	11.41	39.40	43.66	-	-	-	-
J1734.3+3858	0.98	FSRQ	LSP	13.27	0.31	-	-	-	-	0.39	12.88	43.56	-
J1740.3+5211	1.38	FSRQ	LSP	13.91	0.32	1.42	12.48	36.98	42.52	-	-	-	-
J1742.2+5947	-	BL Lac	ISP	-	-	-	-	-	-	−0.50	-	-	44.38
J1743.9+1934	0.08	BL Lac	HSP	15.23	−1.28	-	-	-	-	−0.65	15.87	48.64	45.11
J1744.3−0353	1.06	FSRQ	LSP	13.26	−0.57	1.29	11.97	37.13	-	-	-	-	-
J1748.6+7005	0.77	BL Lac	LSP	14.57	−0.49	-	-	-	-	−0.24	14.81	47.98	45.33
J1749.1+4322	-	BL Lac	LSP	-	-	-	-	-	-	0.11	-	-	43.81
J1751.5+0939	0.32	BL Lac	LSP	13.85	0.03	1.08	12.77	37.67	42.70	-	-	-	-
J1800.5+7827	0.68	BL Lac	LSP	13.76	−0.23	1.09	12.67	38.67	42.71	0.41	13.35	43.42	44.06
J1806.7+6949	0.05	BL Lac	ISP	14.20	−0.66	0.04	14.16	43.52	43.87	−0.05	14.25	44.16	44.05
J1813.6+3143	0.12	BL Lac	ISP	14.81	−0.75	-	-	-	-	−0.58	15.39	48.12	44.78
J1824.2+5649	0.66	BL Lac	LSP	13.73	0.23	0.81	12.92	40.66	43.79	0.56	13.17	42.37	44.28
J1829.6+4844	0.69	SSRQ	LSP	13.32	−0.89	0.76	12.56	41.36	-	-	-	-	-
J1848.4+3216	0.80	FSRQ	LSP	13.28	0.77	-	-	-	-	−0.15	13.43	47.31	-
J1849.2+6705	0.66	FSRQ	LSP	13.84	0.25	-	-	-	-	0.89	12.95	39.76	43.62
J1852.4+4856	1.25	FSRQ	LSP	13.53	0.58	-	-	-	-	1.17	12.36	38.17	-
J2000.0+6509	0.05	BL Lac	HSP	16.19	−0.84	-	-	-	-	−0.34	16.53	46.35	-
J2001.8+7041	0.25	BL Lac	HSP	13.52	−0.18	-	-	-	-	−0.95	14.47	50.83	-
J2005.2+7752	0.34	BL Lac	LSP	14.07	−0.60	1.12	12.94	37.51	42.08	0.29	13.78	43.36	43.75
J2022.5+7612	0.59	BL Lac	ISP	14.51	−0.28	-	-	-	-	0.38	14.14	43.24	-
J2031.8+1223	1.22	BL Lac	LSP	14.04	−0.20	-	-	-	-	0.98	13.06	39.85	-
J2035.3+1055	0.60	FSRQ	ISP	13.90	0.22	-	-	-	-	0.43	13.47	43.13	44.01
J2115.4+2933	1.51	FSRQ	LSP	13.33	0.25	-	-	-	-	−0.84	14.17	52.54	-
J2116.1+3339	1.60	BL Lac	HSP	15.35	−0.17	-	-	-	-	−1.05	16.40	54.14	-
J2121.0+1901	2.18	FSRQ	ISP	13.33	0.11	-	-	-	-	−0.35	13.68	49.32	-
J2123.6+0533	1.94	FSRQ	LSP	13.98	−0.92	1.18	12.79	38.55	-	-	-	-	-
J2143.5+1744	0.21	FSRQ	ISP	14.23	0.78	-	-	-	-	0.48	13.75	42.18	43.41
J2152.4+1735	0.87	BL Lac	LSP	13.83	−1.27	-	-	-	-	−0.52	14.35	49.57	-
J2202.7+4217	0.07	BL Lac	LSP	14.10	−0.36	0.86	13.24	38.59	41.72	-	-	-	-
J2203.4+1725	1.08	FSRQ	LSP	14.05	0.18	-	-	-	-	0.12	13.93	45.75	45.26
J2203.7+3143	0.29	FSRQ	LSP	14.52	2.25	0.83	13.70	42.23	-	-	-	-	-
J2212.0+2355	1.13	FSRQ	LSP	13.31	−0.10	-	-	-	-	0.41	12.89	43.16	-
J2217.0+2421	0.50	BL Lac	LSP	14.28	−0.68	-	-	-	-	0.82	13.46	39.83	43.14
J2225.8−0454	1.40	FSRQ	LSP	13.24	−0.44	1.20	12.04	38.70	43.88	-	-	-	-
J2229.7−0833	1.56	FSRQ	LSP	13.89	1.00	1.20	12.69	39.26	42.77	-	-	-	-
J2232.5+1143	1.04	FSRQ	LSP	13.42	0.41	1.19	12.23	38.99	43.33	-	-	-	-
J2236.3+2829	0.79	BL Lac	LSP	14.08	−0.13	0.78	13.30	40.91	-	0.72	13.36	41.32	-
J2250.1+3825	0.12	BL Lac	-	15.54	−0.90	-	-	-	-	−0.97	16.51	50.96	-
J2251.9+4031	0.23	BL Lac	ISP	14.25	0.03	-	-	-	-	−0.74	14.99	49.54	-
J2254.0+1608	0.86	FSRQ	LSP	13.64	0.76	1.52	12.12	37.12	42.82	1.07	12.57	40.26	43.71
J2311.0+3425	1.82	FSRQ	LSP	13.72	0.47	-	-	-	-	0.06	13.66	46.84	45.66
J2321.9+2732	1.25	FSRQ	LSP	13.63	−0.58	-	-	-	-	−0.07	13.70	47.00	-
J2321.9+3204	1.49	FSRQ	LSP	13.59	0.36	-	-	-	-	0.67	12.92	41.76	-
J2322.5+3436	0.10	BL Lac	HSP	15.27	−0.27	-	-	-	-	−0.87	16.14	50.06	-

it can underestimate the real Doppler factor (see detailed discussions in Sect. 2.2).

2.2 Results

The scatters of $\nu_{\rm S,p}$ versus $\delta_{\rm var}$ and $\nu_{\rm S,p}$ versus $\delta_{\rm eq}$ are plotted in Figure 1. The synchrotron peak frequency $\nu_{\rm S,p}$ is negatively correlated with Doppler factor for both $\delta_{\rm var}$ and $\delta_{\rm eq}$, with the correlation coefficient of Spearman rank correlation test $\rho = -0.48$ and the chance probability $P = 8.7 \times 10^{-5}$ for $\delta_{\rm var}$, and $\rho = -0.30$ and $P = 3.4 \times 10^{-4}$ for $\delta_{\rm eq}$. In the right panel of Figure 1, there is no clear trend for each type of source. The global correlation can be a result of different locations of HBLs and other types of sources (see the following for a possible explanation). As a result of Doppler boosting, we have $\nu_{\rm S,p} = \delta\nu_{\rm S,int}$. Thus, the observational peak frequency is expected to be positively correlated with the Doppler factor. The opposite trends shown in Figure 1 imply some physical connections between the peak frequency and Doppler factor.

In order to identify the physical connections, we apply linear regressions to fit the Doppler-corrected peak frequency and Doppler factor. The input uncertainties are set to 0.3 dex for both sides (Ackermann et al. 2015; Hovatta et al. 2009). The fitting results are

$$\log \nu_{\rm S,int} = (-2.54 \pm 0.54) \log \delta_{\rm var} + (15.32 \pm 0.56) \quad (1)$$

with intrinsic scatter 0.14 dex, and

$$\log \nu_{\rm S,int} = (-1.83 \pm 0.14) \log \delta_{\rm eq} + (14.09 \pm 0.07) \quad (2)$$

with intrinsic scatter 0.44 dex. The two linear relations are generally consistent with each other, but the latter has a sightly flatter slope (Fig. 2). Lähteenmäki & Valtaoja (1999) proposed that during the quiescent state of total flux density, the intrinsic brightness temperature was smaller than the equipartition value. $\delta_{\rm eq}$ has been estimated through a single very long baseline interferometry (VLBI) observation, thus it underestimates the real Doppler factor for the sources which passed the maximum phase of a shock development. This effect may cause the flatter slope between $\nu_{\rm S,int}$ and $\delta_{\rm eq}$.

In the right panel of Figure 2, HBLs clearly show a different trend from other types of sources. Excluding HBLs, the correlation coefficient between peak frequency and Doppler factor changes to -1.42, which is much flatter than -1.83 in Equation (2). This implies that the underestimation of the real Doppler factor is more serious for FSRQs and LBLs than for HBLs. One interpretation is that FSRQs and LBLs are always located at higher redshift and are more variable.

3 JET POWER

Meyer et al. (2011) suggested kinetic jet power as an essential feature in blazar classifications. We thus build a cross-matched sample from the 3LAC clean sample and the sample of Nemmen et al. (2012). This cross-matched sample contains 113 FSRQs and 104 BL Lacs. The distribution of kinetic jet power for this sample is plotted in Figure 3. The dichotomy between FSRQs and BL Lacs is obviously shown. The Kolmogorov-Smirnov (K-S) test confirms that these two subclasses are drawn from distinct samples with $D = 0.67$ and probability $P = 1.9 \times 10^{-22}$. Because the material energy loading in jets is also boosted by the jet speed with a factor of Γ^2 (e.g. Celotti & Ghisellini 2008), the distribution of kinetic jet power is also influenced by the Doppler factor. We estimate the material energy in the comoving frame (hereafter intrinsic jet power) with $P_{\rm j,int} = P_{\rm j}/\Gamma^2 \sim P_{\rm j}/\delta^2$. The sample with $\delta_{\rm var}$ estimation has 33 FSRQs and 20 BL Lacs, while 40 FSRQs and 44 BL Lacs have $\delta_{\rm eq}$ estimations. The details of these two samples are also combined in Table 1. The distributions of $P_{\rm j,int}$ calculated by two groups of δ are plotted in Figure 4. BL Lacs and FSRQs roughly have the same range of $P_{\rm j,int}$. The null hypotheses that FSRQs and BL Lacs are drawn from the same distribution are not rejected by the K-S tests, with $D = 0.34$, probability $P = 0.09$ and $D = 0.18$, probability $P = 0.49$ for the intrinsic jet power, calculated by $\delta_{\rm var}$ and $\delta_{\rm eq}$, respectively. FSRQs and BL Lacs are suggested to be located in distinct accretion regimes (e.g., Ghisellini et al. 2011). If this is the case, then our results indicate that the material energy of a jet is independent of the accretion mode. The distinctions of jet power between FSRQs and BL Lacs are mainly caused by the jet speed which is related to the jet acceleration processes or the gas environments in the host galaxies. Therefore, the assumption that the jet power is proportional to the accretion rate (e.g. Ghisellini & Tavecchio 2008) should be used carefully.

4 BLAZAR SEQUENCE

Nieppola et al. (2008) found that the negative correlation between the peak frequency and luminosity became positive after the Doppler boosting was corrected. Thus we examine the Doppler-corrected blazar sequence for our samples. The Doppler-corrected intrinsic bolometric luminosity is calculated as follows. The isotropic luminosity $L_{\rm iso}$ is first obtained by combing the synchrotron peak luminosity and IC peak luminosity, where the synchrotron peak luminosity $L_{\rm S} = \nu_{\rm S,p} L_{\rm S,p} = 4\pi {d_L}^2 \nu^{'}_{\rm S,p} F^{'}_{\rm S,p}$ and IC peak luminosity $L_{\rm IC} = \nu_{\rm IC,p} L_{\rm IC,p} = 4\pi {d_L}^2 \nu^{'}_{\rm IC,p} F^{'}_{\rm IC,p}$. The peak flux of synchrotron emission $F^{'}_{\rm S,p}$ and the peak frequency of IC process $\nu^{'}_{\rm IC,p}$ are estimated through the empirical relations from Abdo et al. (2010). The flux of IC peak $F^{'}_{\rm IC,p}$ is estimated by extrapolating the LAT flux to IC peak. Because the radiation of the blazar is highly anisotropic, the realistic solid angle of the anisotropic emission is $2\pi(1 - \cos\theta_{\rm j})$ corresponding to the jet opening angle $2\theta_{\rm j}$. However, the isotropic luminosity is calculated assuming the solid angle 4π. The deviation is $(1 - \cos\theta_{\rm j})/2 \sim \theta_{\rm j}^2/4 \sim 1/4\delta^2$ for small opening angles. Moreover, according to a moving, isotropic jet model, the boosting factor of the luminosity is consid-

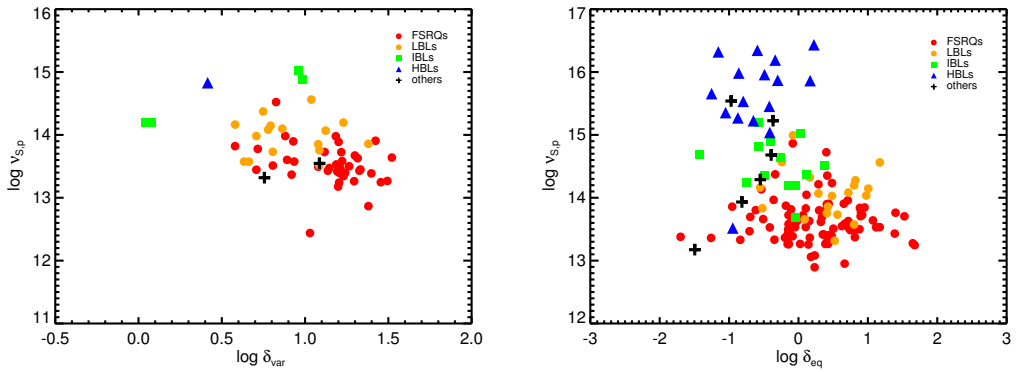

Fig. 1 The correlations between the observational synchrotron peak frequency and the Doppler factor. Different classifications are represented by different symbols as labeled. *Left panel*: $\delta_{\rm var}$ versus $\nu_{\rm S,p}$. *Right panel*: $\delta_{\rm eq}$ versus $\nu_{\rm S,p}$.

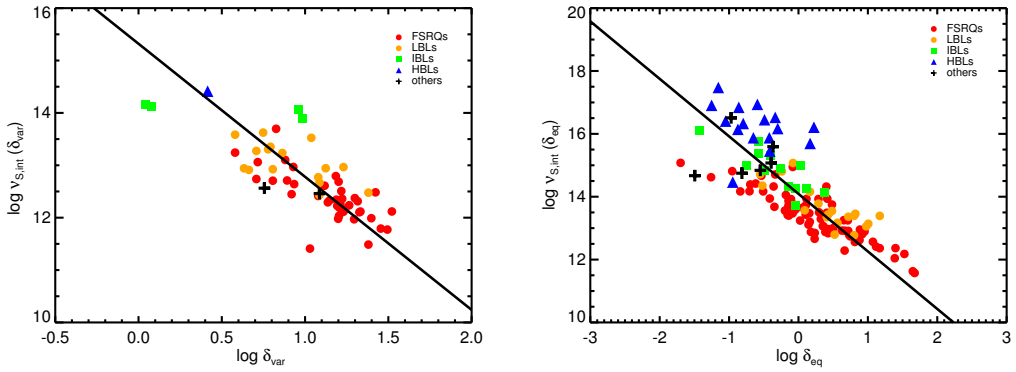

Fig. 2 The correlations between the Doppler-corrected synchrotron peak frequency and the Doppler factor. Different classifications are represented by different symbols as labeled. *Left panel*: $\delta_{\rm var}$ versus $\nu_{\rm S,int}$; *Right panel*: $\delta_{\rm eq}$ versus $\nu_{\rm S,int}$. The solid lines show the best fit.

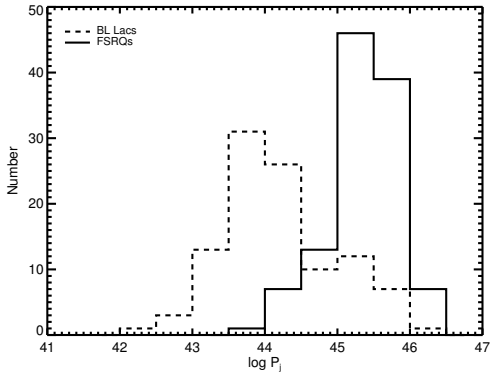

Fig. 3 The distribution of kinetic jet power. The solid lines correspond to FSRQs while the dashed lines correspond to BL Lacs.

ered to be $\nu L_\nu = \delta^{4+\alpha}\nu^{\rm iso}L_\nu^{\rm iso}$, where $L_\nu^{\rm iso}$ is the intrinsic monochromatic luminosity in the comoving frame, L_ν is beamed monochromatic luminosity and α is the spectral index, which is taken as 1 around the peak (Urry & Padovani 1995; Nieppola et al. 2008). Thus the intrinsic bolometric luminosity is estimated to be $L_{\rm bol} \sim L_{\rm iso}/4\delta^7$.

Apparently, positive correlations are shown between $\nu_{\rm S,int}$ and $L_{\rm bol}$ in Figure 5. However, after removing the common dependence on the Doppler factor of these two parameters with the partial Kendall's τ correlation test (Akritas & Siebert 1996), no correlation exists between them. The correlation coefficients τ and the chance prob-

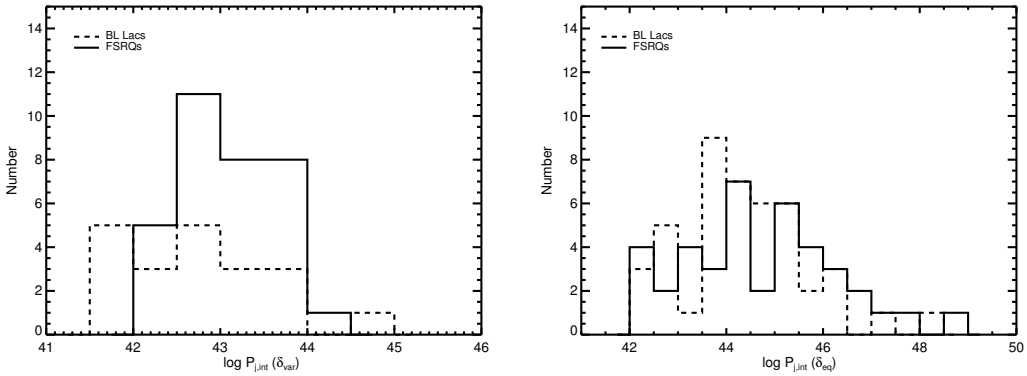

Fig. 4 The distributions of intrinsic jet power. The solid lines correspond to FSRQs, while the dashed lines correspond to BL Lacs. The left panel is calculated by $\delta_{\rm var}$ while the right panel is calculated by $\delta_{\rm eq}$.

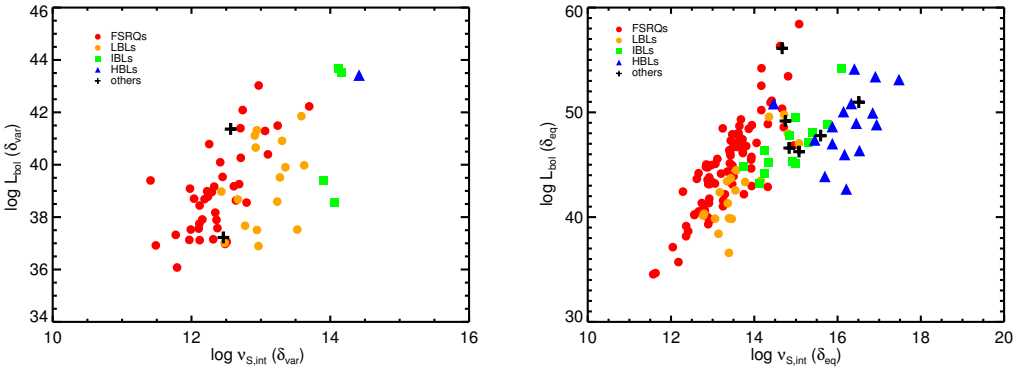

Fig. 5 The correlations between Doppler-corrected synchrotron peak frequency and bolometric luminosity. Different classifications are represented by different symbols as labeled. The left panel is calculated by $\delta_{\rm var}$ while the right panel is calculated by $\delta_{\rm eq}$.

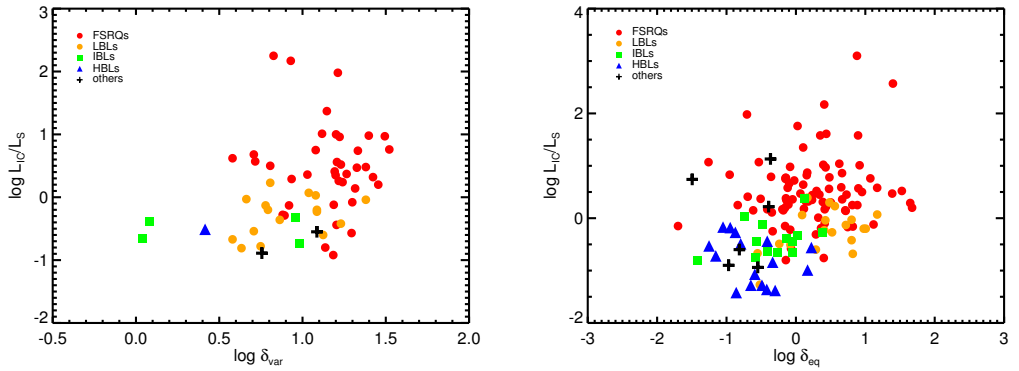

Fig. 6 The correlations between CD and Doppler factor. Different classifications are represented by different symbols as labeled. The left panel: $\delta_{\rm var}$ versus CD; The right panel: $\delta_{\rm eq}$ versus CD.

abilities P are 0.01 and 0.87 respectively for the parameters calculated with $\delta_{\rm var}$, and 0.04 and 0.24 respectively for those calculated with $\delta_{\rm eq}$. The anti-correlation between observational peak frequency and luminosity disappears after the Doppler boosting is corrected. Thus, the blazar sequence is a result of the Doppler boosting. Ghisellini et al. (1998) explained the anti-correlation between the observational peak frequency and luminosity as a consequence of the anti-correlation between the break energy of the electron spectrum and the strength of EC radiation, and proposed that the increased cooling from the external photons led to both decrease of the peak frequency and increase of the luminosity. Our results indicate that the cooling effect seems unimportant for determining the peak frequency because the intrinsic luminosity has no correlation with peak frequency. Recently, Chen (2014) found a significant cor-

relation between the synchrotron peak frequency and the curvature of SEDs. Their result also implied that the break energy of electron spectrum $\gamma_{\rm b}$ was mainly determined by the particle acceleration process (also see the reference therein). The different $\gamma_{\rm b}$ then results in different peak frequency. On the other hand, the different magnetic fields of the emission region also result in various observational features related to the peak frequency.

Similar to Figures 1 and 2, HBLs show an additional track in the right panel of Figure 5. This could be caused by different physical features between HBLs and other blazars, such as radiative efficiency or the radiation mechanism. We examine the correlation between $\nu_{\rm S,int}$ and $L_{\rm bol}$ for the sample excluding HBLs. The result of the partial correlation test still shows no correlation existing between these two parameters, with $\tau = 0.07$ and $P = 0.07$. For HBLs alone, there is also no correlation between $\nu_{\rm S,int}$ and $L_{\rm bol}$, with $\tau = 0.05$ and $P = 0.7$. On the other hand, the additional track of HBLs can also be caused by the underestimation of the real Doppler factor for $\delta_{\rm eq}$ (Lähteenmäki & Valtaoja 1999, Sect. 2.2). Because the current sample of $\delta_{\rm var}$ has few HBLs, a completed sample of $\delta_{\rm var}$ derived from a radio monitoring program, e.g., OVRO (Richards et al. 2011), would help to confirm this trend in the future.

5 EXTERNAL COMPTON EMISSION

Meyer et al. (2012) found a correlation between CD and δ for the very high power sources (including radio galaxies and blazars). They explained that the high energy components of these sources were dominated by the EC process rather than the synchrotron self-Compton (SSC) process. They then suggested this correlation can be used to examine the EC dominance of blazars. We plot the scatters of CD and δ in Figure 6 for our samples. There are weak correlations between CD and δ for all sources, with $\rho = 0.37$, $P = 3.4 \times 10^{-3}$ for $\delta_{\rm var}$, and $\rho = 0.32$, $P = 1.1 \times 10^{-4}$ for $\delta_{\rm eq}$. More importantly, HBLs have the same trend on the CD-δ plane as LBLs and FSRQs (right panel of Fig. 6).

For the SSC process, if the ratio of synchrotron energy density to magnetic field energy density $u_{\rm syn}/u_B \simeq {\rm CD} \propto \gamma_{\rm b}^3 N(\gamma_{\rm b})/R^2$ is independent of Doppler factor (where $N(\gamma_{\rm b})$ is the electron number at the break energy $\gamma_{\rm b}$ and R is the radius of the emission region; see e.g. Finke 2013), then the correlation of CD and δ only exists for the EC process. However, if either the electron distribution or the radius of emission region changes with the bulk Lorentz factor (it seems impossible for the viewing angle to be correlated with these parameters by coincidence), then the correlation between CD and δ is also expected for the SSC process. As a result of the adiabatic expansion, the radius of the emission region is the cross sectional radius of a cone. We have $R \sim r\theta_{\rm j} \sim r/\Gamma$, where r is the distance between the emission region and the central nucleus and $\theta_{\rm j}$ is the opening angle of the jet (e.g., Sikora et al. 2009). Thus the increase of Γ results in the decrease of R. As a result, CD increases as Γ increases. This means that the correlation between CD and δ also exists for the SSC dominant sources. However, if CD being correlated with δ is not a unique feature of EC emission, then this trend will be unsuitable for examining the EC dominance.

6 DISCUSSIONS

If the viewing angles of the γ-ray detected blazars are small, then the bulk Lorentz factors Γ are approximately equal to the Doppler factors δ (Savolainen et al. 2010). Thus the trends found for the Doppler factor are mainly determined by the bulk Lorentz factor. Our correlation analyses between the Doppler-corrected peak frequency and bolometric luminosity indicate that the electron acceleration processes or the magnetic field of the emission region determines the peak frequency. The correlation between the peak frequency and Doppler factor further represents a connection between peak frequency and bulk Lorentz factor. Moreover, the distinction of the kinetic jet power is also caused by the bulk Lorentz factor. Therefore, we can expect that the differences in blazars are determined by a single parameter, i.e., the bulk Lorentz factor. Meyer et al. (2011) discussed the possibility of structured jets with velocity gradients. The radiations of the sources with large viewing angles are dominated by the slow regions. Then, varying the viewing angles forms an observational sequence. In a similar way, different bulk Lorentz factors for individual blazars can directly lead to the same observational appearance.

One scenario to explain the different bulk Lorentz factors was suggested by Potter & Cotter (2013b). They explained that the bulk Lorentz factor was governed by the accretion rate and the black hole masses were similar for all blazars. The higher accretion rate leads to smaller mass loading into the jets, so that a larger fraction of accretion power is converted to accelerate the jet. Finally, this process results in a larger bulk Lorentz factor. Our results seem to rule out this scenario because the material energy loading in jets (i.e., the intrinsic jet power) is independent of the accretion rate (see Sect. 3). Chai et al. (2012) found a significant correlation between the bulk Lorentz factor and black hole mass, but no correlation between the bulk Lorentz factor and Eddington ratio. Their results also suggest that the bulk Lorentz factor is independent of the accretion rate, but governed by the black hole mass. Potter & Cotter (2013a) also presented another scenario to unify the jet physics. They assumed that the radius of the transition region (where the jet comes into equipartition between magnetic field energy and particle energy, and dominates the optically thin synchrotron emission) scales linearly with black hole mass. Therefore, the larger black hole mass leads to a farer transition region from the central black hole. This further results in lower magnetic field strength and finally produces lower synchrotron peak frequency. Based on another assumption that the intrinsic jet power has a fixed fraction of the Eddington luminosity (i.e. the intrinsic jet power is independent of accretion rate), they derived a relation between the synchrotron peak frequency and the black hole

mass in the form $\nu_{\rm S,int} \propto M_{\rm BH}^{-1/2}$. Observationally, the anti-correlation between peak frequency and black hole mass has been found by, e.g., Chen & Bai (2011). When combining this relation with $\Gamma \propto M_{\rm BH}^{0.2}$ found by Chai et al. (2012), we have $\nu_{\rm S,int} \propto \Gamma^{-2.5}$. This relation agrees well with our findings presented in Equations (1) and (2). Therefore, the SEDs of blazars are mainly determined by the black hole mass, but not the luminosity (Ghisellini et al. 1998), accretion rate (Ghisellini et al. 2009) or orientation (Meyer et al. 2011).

7 CONCLUSIONS

In this paper, we obtain two groups of Doppler factors estimated through two independent methods and we aim to identify whether the Doppler factor determines the observational differences of blazars. Significant correlations are found between the Doppler factors and the indicator of the SED classification, i.e., observational synchrotron peak frequency. After correcting the Doppler boosting, the intrinsic peak frequency shows uniform linear relations with two groups of Doppler factors. In addition, we find the distinction of jet power is mainly caused by the different Doppler factors for different subclasses. The negative correlation between the peak frequency and the observational isotropic luminosity disappears after the Doppler boosting is corrected. All of these results confirm that the Doppler factor (physically the bulk Lorentz factor) determines the observational differences of blazars. Furthermore, the black hole mass plays an important role in controlling the bulk Lorentz factor and SED of blazars. Moreover, we find the correlation between the CD and the Doppler factor exists for all types of blazars, thus this correlation is unsuitable for examining the dominance of EC emission. The correlation between CD and Doppler factor can be explained for the SSC process if the radius of the emission region decreases as the bulk Lorentz factor increases.

Acknowledgements We thank the anonymous referee for his/her useful comments. We are also grateful to Yi-Bo Wang, Liang Chen and Neng-Hui Liao for their useful discussions which greatly improved this manuscript. This research is supported by the Strategic Priority Research Program of the Chinese Academy of Sciences - The Emergence of Cosmological Structures (grant No. XDB09000000), the Key Research Program of the Chinese Academy of Sciences (grant No. KJZD-EW-M06), and the National Natural Science Foundation of China (NSFC) through NSFC-11133006 and 11361140347. J. Mao is supported by the Hundred-Talent Program of Chinese Academy of Sciences.

References

Abdo, A. A., Ackermann, M., Agudo, I., et al. 2010, ApJ, 716, 30
Acero, F., Ackermann, M., Ajello, M., et al. 2015, ApJS, 218, 23
Ackermann, M., Ajello, M., Atwood, W. B., et al. 2015, ApJ, 810, 14
Akritas, M. G., & Siebert, J. 1996, MNRAS, 278, 919
Celotti, A., & Ghisellini, G. 2008, MNRAS, 385, 283
Chai, B., Cao, X., & Gu, M. 2012, ApJ, 759, 114
Chen, L. 2014, ApJ, 788, 179
Chen, L., & Bai, J. M. 2011, ApJ, 735, 108
Finke, J. D. 2013, ApJ, 763, 134
Fossati, G., Maraschi, L., Celotti, A., Comastri, A., & Ghisellini, G. 1998, MNRAS, 299, 433
Ghisellini, G., Celotti, A., Fossati, G., Maraschi, L., & Comastri, A. 1998, MNRAS, 301, 451
Ghisellini, G., Maraschi, L., & Tavecchio, F. 2009, MNRAS, 396, L105
Ghisellini, G., Padovani, P., Celotti, A., & Maraschi, L. 1993, ApJ, 407, 65
Ghisellini, G., & Tavecchio, F. 2008, MNRAS, 387, 1669
Ghisellini, G., Tavecchio, F., Foschini, L., & Ghirlanda, G. 2011, MNRAS, 414, 2674
Giommi, P., Padovani, P., Polenta, G., et al. 2012, MNRAS, 420, 2899
Hovatta, T., Valtaoja, E., Tornikoski, M., & Lähteenmäki, A. 2009, A&A, 494, 527
Komatsu, E., Dunkley, J., Nolta, M. R., et al. 2009, ApJS, 180, 330
Kovalev, Y. Y., Aller, H. D., Aller, M. F., et al. 2009, ApJ, 696, L17
Lähteenmäki, A., & Valtaoja, E. 1999, ApJ, 521, 493
Linford, J. D., Taylor, G. B., Romani, R. W., et al. 2012, ApJ, 744, 177
Lister, M. L., Aller, M. F., Aller, H. D., et al. 2015, ApJ, 810, L9
Lister, M. L., Homan, D. C., Kadler, M., et al. 2009a, ApJ, 696, L22
Lister, M. L., Cohen, M. H., Homan, D. C., et al. 2009b, AJ, 138, 1874
Meyer, E. T., Fossati, G., Georganopoulos, M., & Lister, M. L. 2011, ApJ, 740, 98
Meyer, E. T., Fossati, G., Georganopoulos, M., & Lister, M. L. 2012, ApJ, 752, L4
Nemmen, R. S., Georganopoulos, M., Guiriec, S., et al. 2012, Science, 338, 1445
Nieppola, E., Valtaoja, E., Tornikoski, M., Hovatta, T., & Kotiranta, M. 2008, A&A, 488, 867
Padovani, P., Giommi, P., & Rau, A. 2012, MNRAS, 422, 48
Potter, W. J., & Cotter, G. 2013a, MNRAS, 431, 1840
Potter, W. J., & Cotter, G. 2013b, MNRAS, 436, 304
Readhead, A. C. S. 1994, ApJ, 426, 51
Richards, J. L., Max-Moerbeck, W., Pavlidou, V., et al. 2011, ApJS, 194, 29
Savolainen, T., Homan, D. C., Hovatta, T., et al. 2010, A&A, 512, A24
Sikora, M., Stawarz, Ł., Moderski, R., Nalewajko, K., & Madejski, G. M. 2009, ApJ, 704, 38
Tavecchio, F., Maraschi, L., & Ghisellini, G. 1998, ApJ, 509, 608
Urry, C. M., & Padovani, P. 1995, PASP, 107, 803